Bio-SAXS determination of Myc-ABCG2 solution structure in the absence or presence of PZ39 was performed using the in-house source Rigaku BioSAXS-2000$^{nano}$ 2D Kratky system. The sample-to-detector distance will be set at 440 mm to get the scattering in the low range (0.01-0.6 Å$^{-1}$) momentum transfer q (=4$\pi$ sin$\theta/\lambda$, where 2$\theta$ is the scattering angle). Exposure time was set to 5-30 minutes per image frame, which is a function of incidence x-ray intensity, protein mass and concentration. To obtain good signal-to-noise ratios, 10 images were taken for each sample and buffer control. 2D images were reduced, averaged, and subtracted to generate the 1D scattering patten using the Rigaku SAXSLab 4.1 program followed by data analysis using BioXTAS RAW package. The radius of gyration (Rg) will be calculated using the Guinier equation $I(q) = Io \exp(-R_g^2 q^2/3)$, where $I_o$ is the extrapolated forward scattering. The pair distance distribution function that is roughly a weighted histogram of atomic-pair distance in the molecule were calculated using GNOM.

**Fig. 1A** shows the purified ABCG2 protein and **1B** shows 1D scattering pattern generated from 2D images using Rigaku SAXSLab 4.1 and further analysis using BioXTAS RAW package. Examination of the normalized Kratky plot suggests that both apo and PZ39-bound ABCG2 are well-folded (**Fig. 1C**). Guinier-fit resulted in a Rg of 33.32 for the apo protein, consistent with the theoretical Rg of 35.62 computed from the cryo-EM structure of apo ABCG2 (PDB ID: 6VXF). In contrast, the Rg for the PZ39-ABCG2 complex is 46.22, much larger than that of the apo ABCG2, indicating that PZ39 binding induced major conformational changes of ABCG2. This Rg of PZ39-bound ABCG2 is also much bigger than the theoretical Rg of 35.88 for the inhibitor Ko143-bound-ABCG2 (PDB ID: 6ETI), suggesting that PZ39 induces unique conformational changes of ABCG2. Paired distance distribution functions were computed, and it also clearly shows a shift to larger paired distances in the PZ39-bound ABCG2 compared with the apo ABCG2 (**Fig. 1E**).

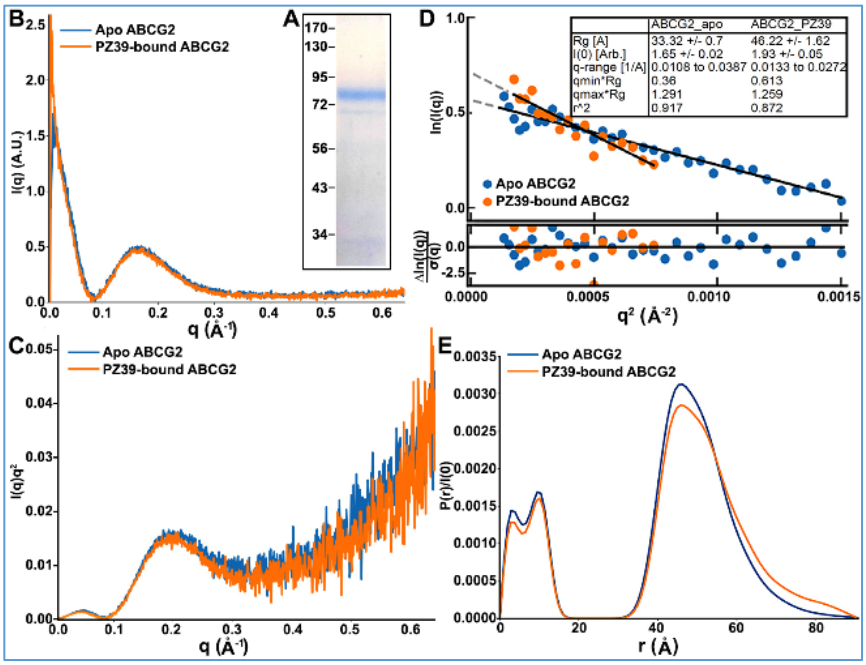


***Figure 1. Purification and bio-SAXS analysis of ABCG2. A****. SDS-PAGE profile of purified Myc-ABCG2 stained with Coomassie blue.* ***B-E.*** *1D scattering pattern (B), Kratky plot (C), Guinier fitting (D), and paired distance distribution function (E) of apo and PZ39-bound ABCG2. The table inset in D shows statistics of data and Guinier-fitting quality.*

***References***


1. Liu, Y.; Peng, H.; Zhang, J.T. Expression profiling of ABC transporters in a drug resistant breast cancer cell line using AmpArray. Mol. Pharmacol. 68:430-438; 2005.
2. Xu, J.; Peng, H.; Chen, Q.; Liu, Y.; Dong, Z.; **Zhang, J.T.** Oligomerization domain of the multidrug resistance-associated transporter ABCG2 and its dominant inhibitory activity. ***Cancer Research*** 67:4373-4381; 2007.
3. Liu, Y.; Yang, Y.; Qi, J.; Peng, H.; Zhang, J.T. Effect of cysteine mutagenesis on the function and disulfide bond formation of human ABCG2. J. Pharm. Exp. Ther. 326:33-40; 2008.
4. Peng, H*.; Dong, Z.*; Qi, J.*; Yang, Y.; Liu, Y.; Li, Z.; Xu, J.; **Zhang, J.T.** A novel two mode-acting inhibitor of ABCG2-mediated multidrug transport and resistance in cancer chemotherapy. ***PLoS One*** 4:e5676; 2009.

5. Peng, H.; Qi, J.; Dong, Z.; **Zhang, J.T**. Dynamic *vs* static ABCG2 inhibitors to sensitize drug resistant cancer cells. ***PLoS One*** 5:e15276; 2010.